

Multichannel nonlinear holography in a two-dimensional nonlinear photonic crystalXinyuan Fang ^{1,2}, Huijun Wang,¹ Haocheng Yang,¹ Zhilin Ye,¹ Yongmei Wang,¹ Yong Zhang ^{1,*},
Xiaopeng Hu,^{1,*} Shining Zhu,¹ and Min Xiao^{1,3,*}¹*National Laboratory of Solid State Microstructures, College of Engineering and Applied Sciences, School of Physics, Nanjing University, Nanjing 210093, China*²*Centre for Artificial-Intelligence Nanophotonics, School of Optical-Electrical and Computer Engineering, University of Shanghai for Science and Technology, Shanghai 200093, China*³*Department of Physics, University of Arkansas, Fayetteville, Arkansas 72701, USA*

(Received 25 February 2020; revised 31 August 2020; accepted 1 September 2020; published 9 October 2020)

To manipulate the wave front of the harmonic wave, nonlinear photonic crystals (NPCs) have been employed in constructing nonlinear holography. Through designing a multi-channel χ^2 structure, nonlinear multiplexing holography is reported here in NPCs. We propose a multi-channel nonlinear holography in an orbital-angular-momentum- (OAM-)multiplexing NPC. In experiment, three images encoded in a single NPC are reconstructed in second-harmonic waves distinctively, when the necessary Fourier-domain OAM-matching conditions are met, respectively. Our method not only conceptually extends nonlinear holography, but also provides a multifunctional platform for high-capacity security storage.

DOI: [10.1103/PhysRevA.102.043506](https://doi.org/10.1103/PhysRevA.102.043506)

The quasi-phase-matching (QPM) theory proposed by Bloembergen provides an effective method to compensate the phase mismatch and enhance the conversion efficiency in the nonlinear light interaction processes [1]. To fulfil the QPM conditions, nonlinear photonic crystals (NPCs), i.e., the domain-modulated LiNbO₃, LiTaO₃, and other ferroelectric materials [2], have been widely investigated in the past several decades [3–6]. Because of the collinear and noncollinear reciprocal vectors in such NPCs, numerous interesting phenomena have been discovered, including nonlinear optical frequency conversion [7], nonlinear Cerenkov radiation [8], conical second-harmonic generation (SHG) [9], nonlinear Talbot self-imaging [10], and so on. By using specially designed NPCs, the concept of holography has also been extended from linear to nonlinear optics [11], leading to a universal method to manipulate arbitrary wave fronts of harmonic waves [12–16]. In experiment, a two-dimensional (2D) NPC with a certain domain structure offers a suitable platform to record a nonlinear hologram. Since the information can only be reconstructed in nonlinear optical fields, the encryption security is improved in comparison to linear holography. However, due to lack of a way to encode various images into a single NPC independently, it remains a great challenge to realize multichannel nonlinear holography.

In order to explore the full capability for information display and enhance the encryption security, multifunctional holograms are highly desired. In linear optical multiplexing holography, additional orthogonal physical dimensions, such as polarization [17,18], wavelength [19–22], time [23], and space [24–27], have been utilized to controllably switch the

holographic images. Unfortunately, in the regime of nonlinear optics, none of the above-mentioned physical dimensions has ever been adopted as an information carrier that is capable to separably reconstruct nonlinear optical images from a χ^2 -modulated NPC plane hologram.

Orbital angular momentum (OAM) [28], due to its inherent orthogonality [29], has emerged as a new degree of freedom of light for boosting classic [30–32] and quantum information capacity [33,34]. Recently, OAM holography for high-density encryption has been experimentally demonstrated in linear optics [35,36]. In nonlinear optical processes, such as SH generation, the traditional phase-matching condition is considered irrelevant to the OAM of lights [37–40], laying a physical barrier to utilize the OAM dimension in nonlinear holography. Here, we propose a Fourier-domain nonlinear OAM-matching mechanism, in which the spiral phase of OAM mode composes an additional phase-matching requirement to control the SH intensity in nonlinear holography. By introducing different OAM orders to encode multiple images, one can controllably switch the holographic images in SH waves and realize OAM-based multichannel nonlinear holography. The sampling in OAM nonlinear holography is governed by the nonlinear OAM conservation law [2]. In the experiment, we employ the popular electrical poling technique [41,42] to fabricate the specially designed nonlinear hologram in a 2D LiTaO₃ NPC. Three independent images encoded in the χ^2 distribution of the 2D NPC will appear individually in the second-harmonic wave when the corresponding OAM-matching condition is met.

A common scheme of nonlinear holography in 2D NPC is to input a fundamental wave (FW) along its z axis and modulate the SH wave front on the x - y plane [upper panel of Fig. 1(a)]. Consider a SHG process in the NPC with dimensions of $W(x) \times H(y) \times L(z)$. The generated SH power can be expressed as $\langle P_{2\omega} \rangle \propto \sin^2 c^2 \left(\frac{\Delta k^x W}{2} \right) \sin^2 c^2 \left(\frac{\Delta k^y H}{2} \right) \sin^2 c^2 \left(\frac{\Delta k^z L}{2} \right)$.

*Corresponding authors: zhangyong@nju.edu.cn; xphu@nju.edu.cn; mxiao@uark.edu

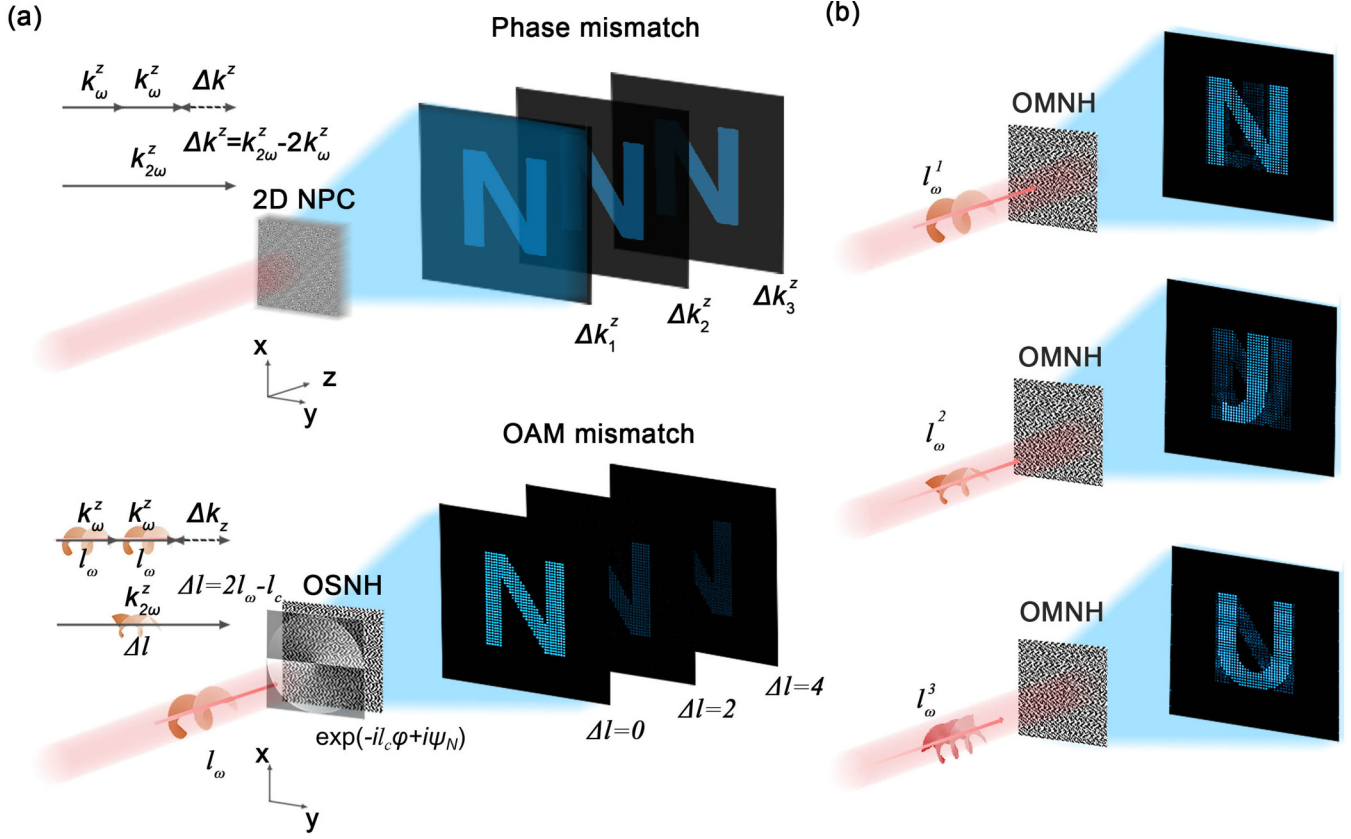


FIG. 1. Conceptual illustrations for Fourier-domain nonlinear OAM matching and multichannel nonlinear holography. (a) Comparison between the phase mismatch and the OAM mismatch in a 2D NPC. (b) Multichannel nonlinear holographic display based on the OAM-multiplexing nonlinear holography.

The domain structure on the x - y plane carries the nonlinear holographic information, which produces the designed SH field through spatial controls of Δk^x and Δk^y under the nonlinear Raman-Nath phase-matching configuration. Considering that the domains along the z direction are unmodulated, and the sample thickness is typically much larger than the coherence length in SH generation, the SH power, as well as, the contrast of SH holographic image are insensitive to $\Delta k^z L$. If multiple images are encoded in this 2D NPC, one cannot distinguish them under the traditional scheme of nonlinear holography.

The conceptual illustration of OAM-matching nonlinear holography is shown in the lower panel of Fig. 1(a). According to the spatial frequency distribution of the spiral phase [35], the OAM dimension can be effectively introduced to encode the SH wave front into the χ^2 distribution of the NPC. After proper sampling, we can obtain the phase-only nonlinear hologram (PONH) of the target SH image [$E_N = \exp(i\psi_N)$]. Then, a spiral phase with $l = -l_c$ [$E_{SPP} = \exp(-il_c\varphi)$] is added on the PONH, resulting in the OAM-selective nonlinear hologram (OSNH),

$$E_N^{\text{OAM-sel}} = E_{SPP} E_N = \exp[i(\psi_N - l_c\varphi)]. \quad (1)$$

When the fundamental beam carrying an OAM of $l = l_\omega$, i.e.,

$$E_\omega(r, \varphi, z) = A_\omega \exp(il_\omega\varphi + ik_\omega^z z) \quad (2)$$

is injected onto the NPC with the above OSNH structure, the electrical field of the generated SH wave in the spatial domain can be expressed as

$$E_{2\omega}(r, \varphi, z) = A_{2\omega} \exp(i\vec{k}_{2\omega}^t \cdot \vec{r} + ik_{2\omega}^z z) = \kappa E_\omega E_\omega E_N^{\text{OAM-sel}}. \quad (3)$$

Here, A_ω and $A_{2\omega}$ are the envelopes of the FW and SH waves, respectively. κ is the nonlinear coupling coefficient. $\vec{k}_{2\omega}^t$ and $k_{2\omega}^z$ are the SH wave vectors along the transverse and longitudinal directions, respectively. Assuming that the pump is undepleted and the field's envelopes vary slowly, $A_{2\omega}$ can be written as

$$A_{2\omega} \approx \kappa \frac{A_\omega^2 [\exp(i\Delta k_z L) - 1]}{i\Delta k_z} \times \exp(i\Delta l\varphi) \exp(i\psi_N - i\vec{k}_{2\omega}^t \cdot \vec{r}). \quad (4)$$

Here, we define

$$\Delta l = 2l_\omega - l_c, \quad (5)$$

as the OAM mismatch in nonlinear optical processes. Then, the electrical field of the SH wave in the spatial frequency domain ($E_{\text{SH}}^{\text{SF}}$) can be expressed as (see Appendix A)

$$E_{\text{SH}}^{\text{SF}} \propto \mathbb{F}\{e^{i\Delta l\varphi}\} \otimes \mathbb{F}\{e^{i(\psi_N - \vec{k}_{2\omega}^t \cdot \vec{r})}\}, \quad (6)$$

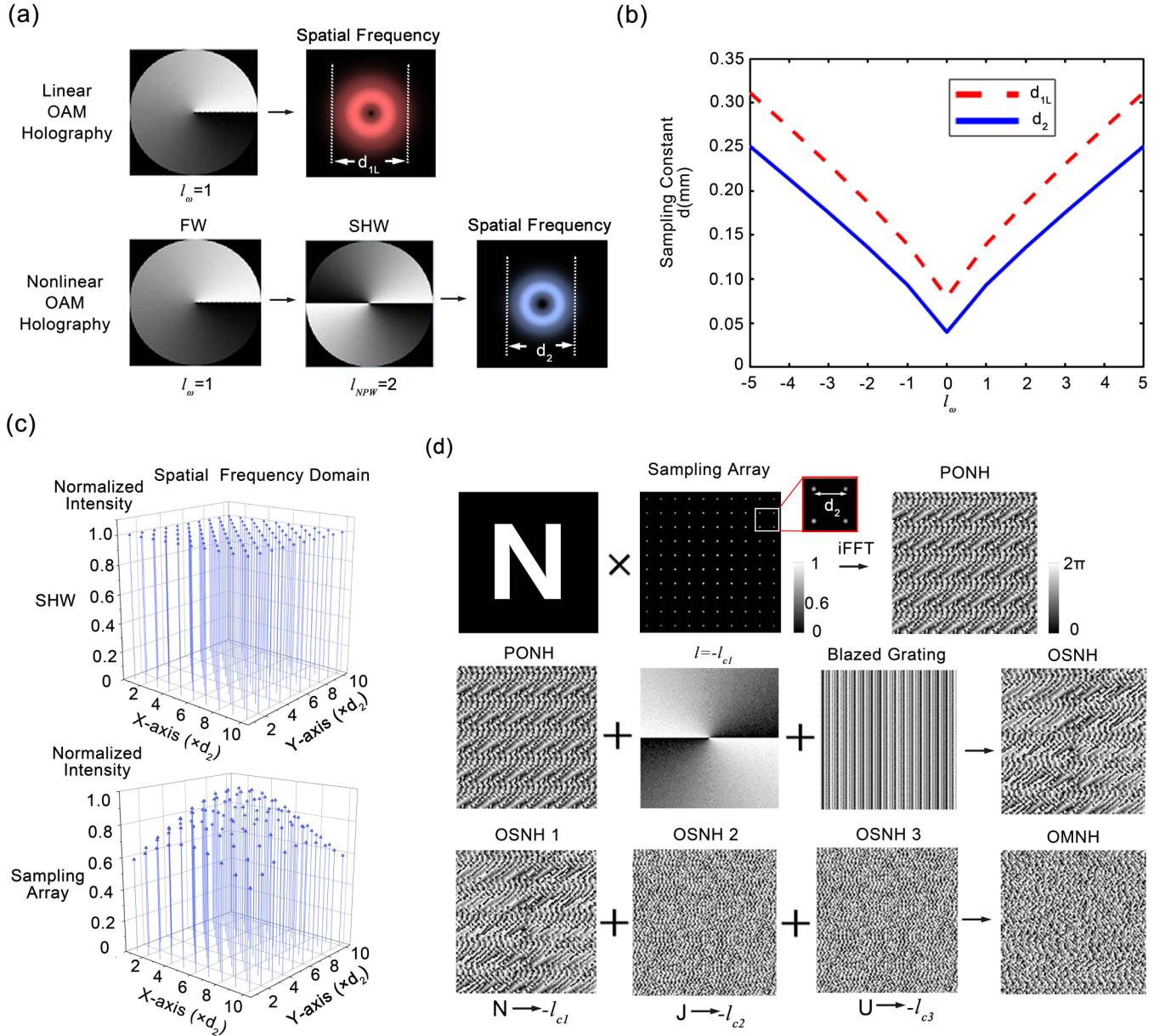


FIG. 2. Principles of OAM nonlinear multiplexing holography. (a) Spatial frequency analysis. (b) Sampling constant calculation for nonlinear OAM holography. (c) Design of sampling array for nonlinear holography. (d) Design principles of the PONH, OSNH, and OMNH.

where \mathbb{F} and \otimes are the symbols of Fourier transformation and convolution, respectively. Only when the OAM-matching condition is met (i.e., $\Delta l = 0$), the target image with Gaussian intensity pixels can be reconstructed distinctively. As shown in Fig. 1(b), OAM selectivity in the OSNH could be applied in multichannel nonlinear holography. Three images (the letters N, J, and U) encoded with different spiral phases ($-l_{c1}$, $-l_{c2}$, and $-l_{c3}$) are multiplexed in an OAM-multiplexing nonlinear hologram (OMNH). When the corresponding OAM-matching condition is met (i.e., $l_\omega^1 = \frac{l_{c1}}{2}$, $l_\omega^2 = \frac{l_{c2}}{2}$, and $l_\omega^3 = \frac{l_{c3}}{2}$), the three letters could be reconstructed in the generated SH wave, respectively.

Proper sampling is critical in order to preserve the encoded spiral phase and guarantee the OAM selectivity [35]. In linear OAM holography, the sampling distance (d_{1L}) is directly

calculated from the spatial frequency of the incident OAM beam. In comparison, two essential differences distinguish the sampling rules in such OAM nonlinear holography. First, the sampling frequency for SH image (d_2) is decided by the spatial frequency of the corresponding SH OAM beam, i.e., $E_{2\omega} = A_{2\omega} \exp(-i2l_\omega\varphi) \exp(-i2k_{2\omega}^z z)$. As shown in Fig. 2(a), the SH OAM order is twice the fundamental one according to the OAM conservation law in nonlinear optical conversion processes [2]. We calculate its distribution in spatial frequency domain and define the sampling constant (d_2) as the 30% of the maximal modulus amplitude without loss of generality (see Appendix B). The relationship between the input FW OAM order and the sampling distance of nonlinear holography is plotted in Fig. 2(b). Here, we use the parameters in our experiment for the calculations.

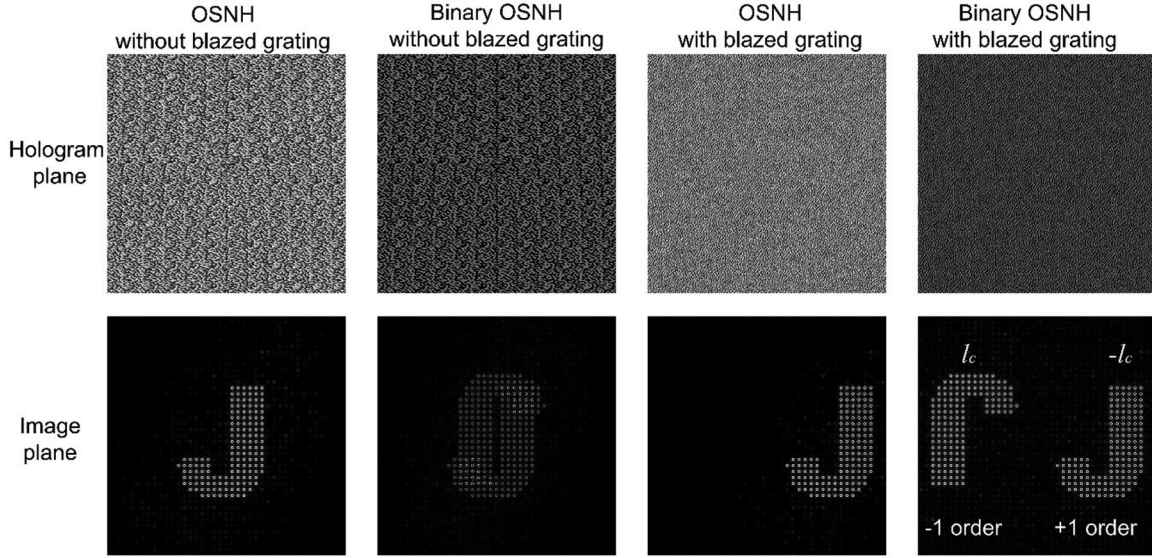


FIG. 3. Effects of binarization and adding a blazed grating function on the OSNHs.

Second, according to the expression of SH conversion efficiency in nonlinear Raman-Nath diffraction $\eta \propto \{\sin c[z(\Delta k^z - \frac{G^2}{2k_{2\phi}})/2]\}^2$ [43], the SH power varies with the involved reciprocal vectors (G). If the intensity distribution of the target SH image is intended to be uniform [upper panel in Fig. 2(c)], the Fourier coefficients of the reciprocal vectors (G) provided by the χ^2 distribution need to be adjusted. This can also be understood since a modified comb function rather than the uniform one as in linear holography [35] is used for sampling in nonlinear holography [lower panel in Fig. 2(c)].

Figure 2(d) shows the procedure to design an OMNH. After the necessary adjustments on the sampling array described above, a PONH of the target image [$E_{\text{PONH}} = \exp(i\psi_{\text{PONH}})$] can be achieved by iterative inverse fast Fourier transformation algorithm [35,36] [Fig. 2(d)]. Then, a spiral phase with $l = -l_c$ is added to achieve the OAM selectivity. In order to eliminate the twin-image effect induced by the binary phase modulation of SH waves (i.e., 0 and π phases from the positive and negative domains, respectively), we add a blazed grating function into the final OSNH $\{E_{\text{OSNH}} = \exp[i(\psi_{\text{PONH}} - l_c\phi + G_b)]\}$. After complex superposition of OSNHs for the letters N, J, and U, the phase term of the complex amplitude distribution, $E_{\text{OMNH}} = \exp[i \cdot \text{angle}(E_{\text{OSNH}}^N + E_{\text{OSNH}}^J + E_{\text{OSNH}}^U)]$, is defined as the OMNH (i.e., the final domain structure encoded in the NPC).

In order to show the effect of the blazed grating function in our design, the images reconstructed from the binary OAM-selective nonlinear holograms with and without blazed grating function are shown in Fig. 3. The OSNH is encoded with a spiral phase plate $l = -l_c$. When inputting a FW of $l_\omega = 0$, a twin image with $l = l_c$ and $l = l_c$ will appear in the spatial frequency domain due to the binarization of OSNH. As such, adding a blazed grating function is a good choice to separate the images.

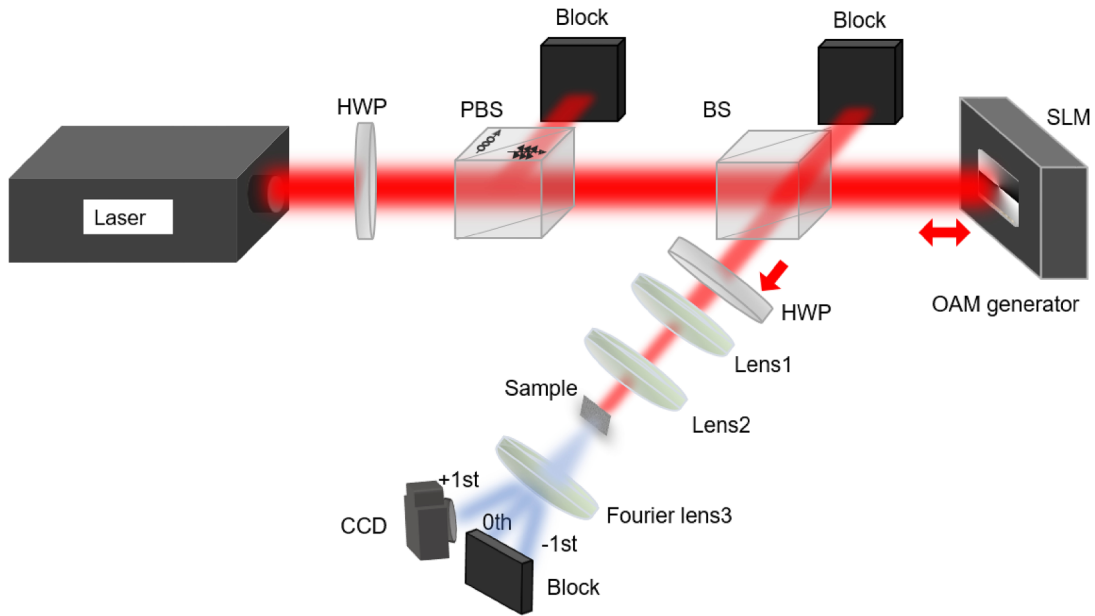
Notably, in the binary OMNH, the blazed grating function is necessary only if the encoded OAM numbers include $-l_c$ and l_c simultaneously. For example, if two images are encoded with $l = 2$ and $l = 4$, the blazed grating is helpful to reduce

the cross talk but not necessary for image selectivity in the OMNH. In our experiment, the letters N and J are encoded with $l = -2$ and $l = 2$, respectively. As a result, the blazed grating function is introduced in the design.

The experimental setup is shown in Fig. 4(a). A 900-nm fundamental beam with a pulse width of 75 fs and a repetition rate of 80 MHz from a Ti:sapphire femtosecond laser (Chameleon, Coherent) passes through a half-wave plate and a polarization beam-splitter to control its power. A spatial light modulator (Holoeye Pluto-2-NIR-011) is used to generate an incident fundamental OAM beam with different topological charges. Then, this fundamental beam is loosely focused by two lenses to an ~ 4 -mm beam waist on the sample. We use a Fourier lens with a focal length of 200 mm to observe the SH images. The charge-coupled device (CCD) camera is put at the +1 order of the binary blazed grating. The samples in our experiment are z -cut LiTaO₃ crystals with dimensions of 4 mm (x) \times 4 mm (y) \times 0.5 mm (z). The domain structure is fabricated by electric-field poling technique at room temperature. Note that z is the propagation direction of the incident FW, and the nonlinear coefficients d_{22} is utilized under our experimental configuration.

Figure 4(b) shows the experimental demonstration of OSNH. The images in the first and second columns illustrate the calculated binary OSNH and the optical microscopic images of the NPC with $\chi^{(2)} = d_{22} \text{sgn}[\sin(\psi_{\text{OSNH}})]$, respectively. When the incident FWs carry no OAM ($l_\omega = 0$), the SH images on the Fourier plane are shown in the third column. Clearly, each pixel has a ring-shaped intensity profile. The corresponding astigmatic transformation patterns [44] in the fourth column suggest that the OAM states encoded in the PONHs of the letters N, J, and U are $l_{c1} = -2$, $l_{c2} = 2$, $l_{c3} = 4$, respectively. As can be seen from the last column of Fig. 4(b), the SH image appears obviously with Gaussian-spot pixel when the FW carries the appropriate OAM state to satisfy the well-defined OAM-matching condition. Notably, the binarization due to the NPC poling technique has no significant effect on the performance of the OAM

(a)



(b)

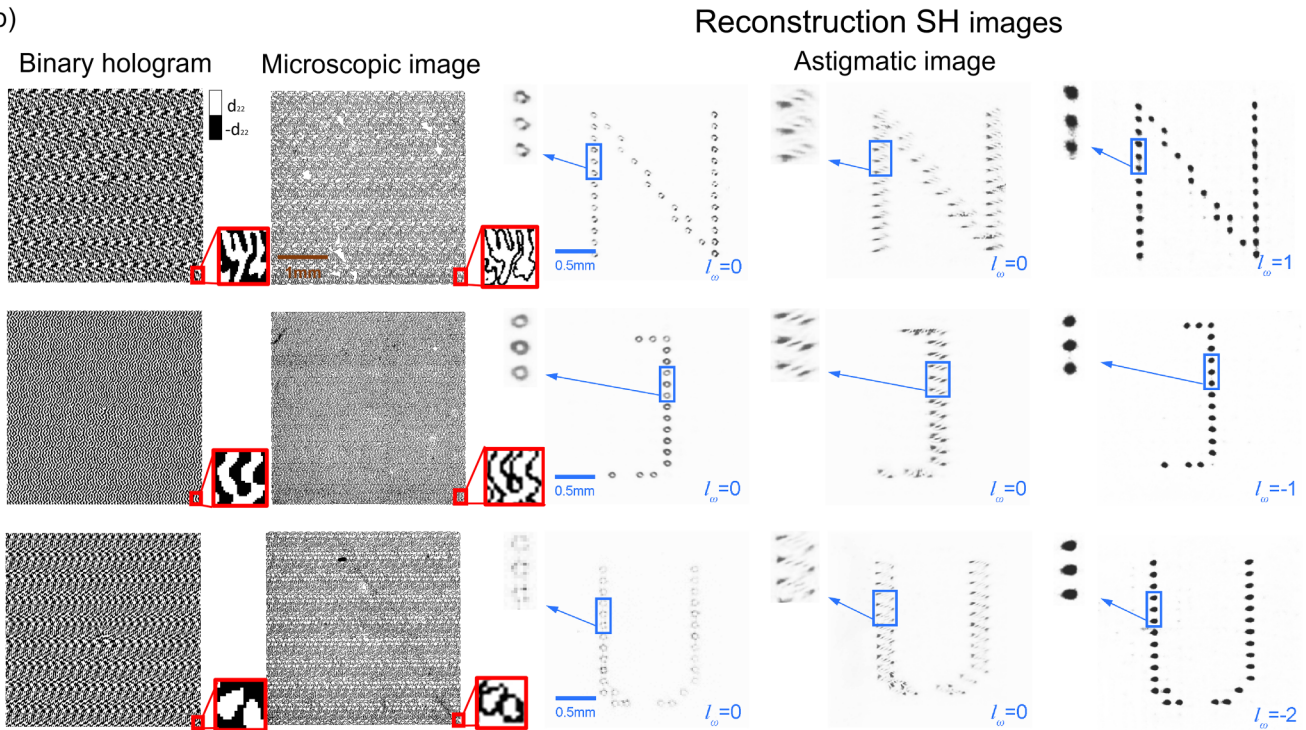


FIG. 4. Experimental demonstration of OSNH. (a) Experimental setup. (b) The structures of the OSNH for the letters N, J, and U encoded with $l_c = -2, 2,$ and 4 are shown in the first (design) and second (experiment) columns. Note that the microscopic images record the domain walls. The third column shows the OAM-mismatched SH images by a fundamental beam with $l_\omega = 0$. The fourth column depicts the corresponding astigmatic images. As shown in the last column, by inputting fundamental beams with $l_\omega = 1, -1,$ and -2 , the letters N, J, and U encoded in the SH waves with Gaussian spot pixels are reconstructed, respectively, when the corresponding OAM-matching condition is satisfied.

nonlinear holography, according to our numerical simulation and experiment.

Based on nonlinear OAM-matching theory, we can achieve OAM-enabled multichannel nonlinear holography in a 2D χ^2 -modulated LiTaO₃ crystal (Fig. 5). The calculated OMNH and the microscopic image of the NPC with

$\chi^{(2)} = d_{22} \text{sgn}[\sin(\psi_{\text{OMNH}})]$ are shown in Fig. 5(a). When the NPC hologram is decoded by a FW with $l_\omega = 0$, the SH image recorded with enhanced CCD sensitivity can be seen in Fig. 5(b). Because of the OAM mismatches, the letters embedded in the SH waves have donut-shaped pixels and relative low intensities, which cannot be well discriminated.

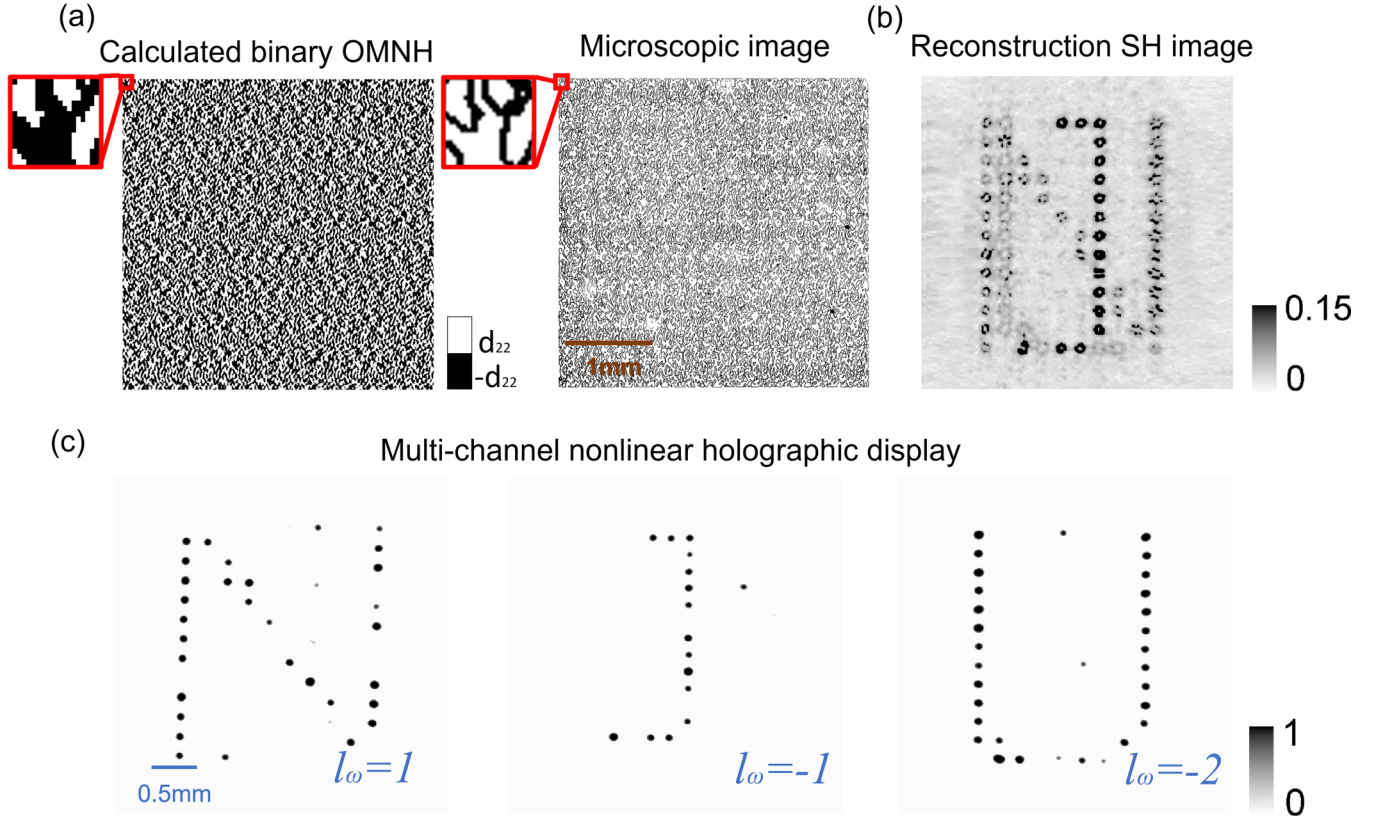


FIG. 5. Experimental demonstration of the OMNH. (a) The designed and experimental structures of the OMNH. (b) The reconstructed SH image by a fundamental beam with $l_\omega = 0$ (i.e., the OAM is mismatched). (c) Three-channel nonlinear holographic displays by using fundamental OAM beams with $l_\omega = 1, -1,$ and -2 to satisfy the OAM-matching conditions, respectively. Notably, the SH intensity in (b) is far lower than those in (c). Notably, the SH intensity in (b) is far lower than those in (c).

As shown in Fig. 5(c), only the fundamental OAM beams with $l_\omega = 1, -1, -2$ can satisfy the corresponding OAM-matching conditions and selectively reconstruct the holographic images. In principle, more SH images could be encoded in a single 2D NPC because of the orthogonality of the OAM orders, which is technically limited by the damage threshold of the used nonlinear crystal and the fabrication precision of domain structure.

In conclusion, we have proposed and experimentally demonstrated multichannel nonlinear holography in 2D χ^2 -encoded NPC by introducing the OAM dimension and making use of its orthogonality. The additional OAM-matching conditions in nonlinear optical processes provide the necessary ability to select various nonlinear holographic images from a single 2D NPC. If the lateral size of the recently developed three-dimensional NPC [5,6] reaches several millimeters, the Fourier-domain OAM-matching technique can, then, be applied for nonlinear volume holography. Notably, the 2D NPC plane hologram has certain unique advantages in compactness and integration for on-chip nonlinear optical applications. We also note that the nonlinear metasurface is another promising platform to realize nonlinear holography under a different mechanism [4,19,45–52]. The combination of the 2D NPC and nonlinear metasurface may provide a potential way to utilize the information channels of the fundamental and SH waves simultaneously. Our

scheme could be further extended to higher-harmonic waves through cascaded nonlinear optical processes in the NPCs [7], leading to wavelength-multiplexing nonlinear holography. Since the NPC has spatially modulated χ^2 rather than χ^1 , the encoded information can only be detected in nonlinear harmonic waves, which provides a useful mechanism for encryption technology. The multichannel nonlinear holography in the OAM multiplexing NPC could significantly boost high-density information security storage and communication capacities.

This work was supported by the National Key R&D Program of China (Grants No. 2017YFA0303703, No. 2016YFA0302500, and No. 2019YFA0705000), the National Natural Science Foundation of China (NSFC) (Grants No. 91950206 and No. 11874213), and Fundamental Research Funds for the Central Universities (Grants No. 021314380105 and No. 021314380177). X.F. acknowledges the funding support from Shanghai Rising-Star Program (Program No. 20QA1404100) and Zhangjiang National Innovation Demonstration Zone (Program No. ZJ2019-ZD-005).

Y.Z. and X.F. proposed the idea and conceived the experiment. Y.Z., S.Z., and M.X. supervised the project. X.F. and H.Y. performed the calculation of nonlinear OAM-multiplexing holograms, Z.Y. and X.H. fabricated the sample, H.W. and Y.W. constructed the optical characterization of the

sample. All authors contributed to the discussions. X.F., Y.Z., and M.X. wrote the paper with contributions from all authors.

APPENDIX A: ELECTRICAL FIELD OF THE SECOND-HARMONIC WAVE IN THE SPATIAL FREQUENCY DOMAIN

In the cylindrical coordinates, we consider a FW $E_1(r, \varphi, z) = A_1 \exp(il_\omega \varphi + ik_\omega^z z)$ and a SH wave $E_2(r, \varphi, z) = A_2 \exp(ik_{2\omega}^z \vec{r} + ik_{2\omega}^z z)$ with A_1 and A_2 being arbitrary envelopes. When the fundamental beam with $l = l_\omega$ is input on the 2D OSNH [$E_N = \exp(i\psi_N)$], assuming that the pump is undepleted, and the field's envelopes vary slowly, the evolution of the SH wave is given by

$$\frac{dA_{2\omega}}{dz} = \kappa A_\omega^2 \exp[i(2l_\omega - l_c)\varphi] \exp[i(2k_\omega^z - k_{2\omega}^z)z] \times \exp(i\psi_N - ik_{2\omega}^z \cdot \vec{r}). \quad (\text{A1})$$

Therefore, the SH wave in the spatial domain can be expressed as

$$A_{2\omega} \approx \kappa \frac{A_\omega^2 [\exp(i \Delta k_z L) - 1]}{i \Delta k_z} \times \exp(i \Delta l \varphi) \exp(i\psi_N - ik_{2\omega}^z \cdot \vec{r}) \quad (\text{A2})$$

Here, $\Delta l = 2l_\omega - l_c$, $\Delta k_z = 2k_\omega^z - k_{2\omega}^z$. As a result, the electrical field of the SH wave in the spatial frequency domain (E_{SH}^{SF}) can be expressed as

$$E_{SH}^{SF} \propto \mathbb{F}\{e^{i \Delta l \varphi}\} \otimes \mathbb{F}\{e^{i(\psi_N - k_{2\omega}^z \cdot \vec{r})}\}. \quad (\text{A3})$$

APPENDIX B: CHARACTERIZATION OF THE SAMPLING CONSTANT FOR THE SECOND-HARMONIC IMAGE

In the cylindrical coordinates, the spiral phase plate with a topological charge l can be expressed as

$$E_{SPP}(r, \varphi) = \text{circ}\left(\frac{r}{R}\right) \exp(il\varphi), \quad (\text{B1})$$

where R is the radius of the spiral phase plate, and r and φ are the radius and azimuthal angle in the polar coordinate system, respectively.

The modulus amplitude of its spatial frequency can be calculated by

$$|E(\rho, \theta)| = \Im |E_{SPP}(r, \varphi)| = \left| \frac{(-1)^{l+1} k}{f} \exp(i\theta) \int_0^R J_1\left(\frac{k}{f} r \rho\right) r dr \right| \quad (\text{B2})$$

where $k = 2\pi/\lambda$ is the wave number and f is the focal length of a Fourier lens. r and ρ are the radii on the hologram plane and the image plane, respectively. Because the modulus amplitude features radial symmetry, the distribution along an arbitrary radius direction can be analyzed by

$$|E(\rho, 0)| = \left| \frac{(-1)^{l+1} k}{f} \int_0^R J_1\left(\frac{k}{f} r \rho\right) r dr \right|. \quad (\text{B3})$$

Without loss of generality, the sampling constant (d), corresponding to the sampling spatial frequency k_g , is defined as 30% of the maximal modulus amplitude throughout this paper.

-
- [1] J. A. Armstrong, N. Bloembergen, J. Ducuing, and P. S. Pershan, *Phys. Rev.* **127**, 1918 (1962).
- [2] X. Hu, Y. Zhang, and S. Zhu, *Adv. Mater.* **32**, 1903775 (2019).
- [3] V. Berger, *Phys. Rev. Lett.* **81**, 4136 (1998).
- [4] N. Segal, S. Keren-Zur, N. Hendler, and T. Ellenbogen, *Nat. Photon.* **9**, 180 (2015).
- [5] D. Wei *et al.*, *Nat. Photon.* **12**, 596 (2018).
- [6] T. Xu *et al.*, *Nat. Photon.* **12**, 591 (2018).
- [7] S. Zhu, Y. Y. Zhu, and N. B. Ming, *Science* **278**, 843 (1997).
- [8] Y. Zhang, Z. D. Gao, Z. Qi, S. N. Zhu, and N. B. Ming, *Phys. Rev. Lett.* **100**, 163904 (2008).
- [9] P. Xu, S. H. Ji, S. N. Zhu, X. Q. Yu, J. Sun, H. T. Wang, J. L. He, Y. Y. Zhu, and N. B. Ming, *Phys. Rev. Lett.* **93**, 133904 (2004).
- [10] Y. Zhang, J. Wen, S. N. Zhu, and M. Xiao, *Phys. Rev. Lett.* **104**, 183901 (2010).
- [11] X. H. Hong, B. Yang, C. Zhang, Y. Q. Qin, and Y. Y. Zhu, *Phys. Rev. Lett.* **113**, 163902 (2014).
- [12] T. Ellenbogen, N. Voloch-Bloch, A. Ganany-Padowicz, and A. Arie, *Nat. Photon.* **3**, 395 (2009).
- [13] B. Yang, X. H. Hong, R. E. Lu, Y. Y. Yue, C. Zhang, Y. Q. Qin, and Y. Y. Zhu, *Opt. Lett.* **41**, 2927 (2016).
- [14] N. V. Bloch, K. Shemer, A. Shapira, R. Shiloh, I. Juwiler, and A. Arie, *Phys. Rev. Lett.* **108**, 233902 (2012).
- [15] D. Wei *et al.*, *Nat. Commun.* **10**, 4193 (2019).
- [16] S. Liu, K. Switkowski, C. Xu, J. Tian, B. Wang, P. Lu, W. Krolikowski, and Y. Sheng, *Nat. Commun.* **10**, 3208 (2019).
- [17] J. F. Heanue, M. C. Bashaw, and L. Hesselink, *Science* **265**, 749 (1994).
- [18] J. P. Balthasar Mueller, N. A. Rubin, R. C. Devlin, B. Groever, and F. Capasso, *Phys. Rev. Lett.* **118**, 113901 (2017).
- [19] D. Wen *et al.*, *Nat. Commun.* **6**, 8241 (2015).
- [20] M. Ozaki, J.-I. Kato, and S. Kawata, *Science* **332**, 218 (2011).
- [21] X. Li *et al.*, *Nat. Commun.* **6**, 6984 (2015).
- [22] X. Li *et al.*, *Sci. Adv.* **2**, e1601102 (2016).
- [23] K. T. P. Lim, H. Liu, Y. Liu, and J. K. W. Yang, *Nat. Commun.* **10**, 25 (2019).
- [24] X. A. Shen, A.-D. Nguyen, J. W. Perry, D. L. Huestis, and R. Kachru, *Science* **278**, 96 (1997).
- [25] G. Makey, O. Yavuz, D. K. Kesim, A. Turnali, P. Elahi, S. Ilday, O. Tokel, and F. O. Ilday, *Nat. Photon.* **13**, 251 (2019).
- [26] P. A. Blanche *et al.*, *Nature (London)* **468**, 80 (2010).
- [27] F. H. Mok, *Opt. Lett.* **18**, 915 (1993).
- [28] L. Allen, M. W. Beijersbergen, R. J. C. Spreeuw, and J. P. Woerdman, *Phys. Rev. A* **45**, 8185 (1992).
- [29] A. M. Yao and M. J. Padgett, *Adv. Opt. Photon.* **3**, 161 (2011).
- [30] J. Wang *et al.*, *Nat. Photon.* **6**, 488 (2012).
- [31] N. Bozinovic, Y. Yue, Y. Ren, M. Tur, P. Kristensen, H. Huang, A. E. Willner, and S. Ramachandran, *Science* **340**, 1545 (2013).

- [32] H. Ren, X. Li, Q. Zhang, and M. Gu, *Science* **352**, 805 (2016).
- [33] A. Mair, A. Vaziri, G. Weihs, and A. Zeilinger, *Nature (London)* **412**, 313 (2001).
- [34] R. Fickler, R. Lapkiewicz, W. N. Plick, M. Krenn, C. Schaeff, S. Ramelow, and A. Zeilinger, *Science* **338**, 640 (2012).
- [35] X. Fang, H. Ren, and M. Gu, *Nat. Photon.* **14**, 102 (2020).
- [36] H. Ren *et al.*, *Nat. Commun.* **10**, 2986 (2019).
- [37] K. Dholakia, N. B. Simpson, M. J. Padgett, and L. Allen, *Phys. Rev. A* **54**, 3742(R) (1996).
- [38] J. Courtial, K. Dholakia, L. Allen, and M. J. Padgett, *Phys. Rev. A* **56**, 4193 (1997).
- [39] Z. Y. Zhou, D. S. Ding, Y. K. Jiang, S. Shi, X. S. Wang, B. S. Shi, and G. C. Guo, *Opt. Express* **22**, 20298 (2014).
- [40] X. Fang, G. Yang, D. Wei, D. Wei, R. Ni, W. Ji, Y. Zhang, X. Hu, W. Hu, Y. Q. Lu, S. N. Zhu, and M. Xiao, *Opt. Lett.* **41**, 1169 (2016).
- [41] S. N. Zhu, Y. Y. Zhu, Z. Y. Zhang, H. F. Wang, H. Shu, J. F. Hong, C. Z. Ge, and N. B. Ming, *J. Appl. Phys.* **77**, 5481 (1995).
- [42] M. Yamada, N. Nada, M. Saitoh, and K. Watanabe, *Appl. Phys. Lett.* **62**, 435 (1993).
- [43] Y. Sheng, Q. Kong, W. Wang, K. Kalinowski, and W. Krolikowski, *J. Phys. B: At. Mol. Opt. Phys.* **45**, 055401 (2012).
- [44] X. Fang, Z. Kuang, P. Chen, H. Yang, Q. Li, W. Hu, Y. Q. Lu, Y. Zhang, and M. Xiao, *Opt. Lett.* **42**, 4387 (2017).
- [45] W. Ye *et al.*, *Nat. Commun.* **7**, 11930 (2016).
- [46] E. Almeida, O. Bitton, and Y. Prior, *Nat. Commun.* **7**, 12533 (2016).
- [47] S. Keren-Zur, L. Michaeli, H. Suchowski, and T. Ellenbogen, *Adv. Opt. Photon.* **10**, 309 (2018).
- [48] T. Pertsch and Y. Kivshar, *MRS Bull.* **45**, 210 (2020).
- [49] Y. Gao, Y. Fan, Y. Wang, W. Yang, Q. Song, and S. Xiao, *Nano Lett.* **18**, 8054 (2018).
- [50] H. Suchowski, K. O'Brien, Z. J. Wong, A. Salandrino, X. Yin, and X. Zhang, *Science* **342**, 1223 (2013).
- [51] M. Kauranen and A. V. Zayats, *Nat. Photon.* **6**, 737 (2015).
- [52] M. Celebrano, X. Wu, M. Baselli, S. Grobmann, P. Biagioni, A. Locatelli, C. D. Angelis, G. Cerullo, R. Osellame, B. Hecht, L. Duo, F. Ciccacci, and M. Finazzi, *Nat. Nanotechnol.* **10**, 412 (2015).